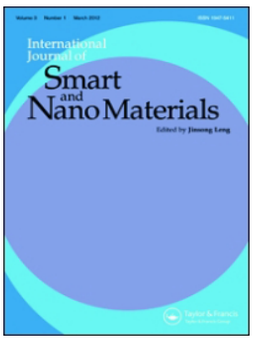

International Journal of Smart and Nano Materials

ISSN: (Print) (Online) Journal homepage: https://www.tandfonline.com/loi/tsnm20

Amino-functionalized magnetic nanoparticles for CO_2 capture

Emanuele Oddo, Ruggiero M. Pesce, Marco Derudi & Luca Magagnin

To cite this article: Emanuele Oddo, Ruggiero M. Pesce, Marco Derudi & Luca Magagnin (2021): Amino-functionalized magnetic nanoparticles for CO_2 capture, International Journal of Smart and Nano Materials, DOI: 10.1080/19475411.2021.1987350

To link to this article: https://doi.org/10.1080/19475411.2021.1987350

© 2021 The Author(s). Published by Informa UK Limited, trading as Taylor & Francis Group.

Published online: 23 Oct 2021.

Submit your article to this journal

Article views: 67

View related articles

View Crossmark data

Full Terms & Conditions of access and use can be found at
https://www.tandfonline.com/action/journalInformation?journalCode=tsnm20

INTERNATIONAL JOURNAL OF SMART AND NANO MATERIALS
https://doi.org/10.1080/19475411.2021.1987350

Taylor & Francis
Taylor & Francis Group

OPEN ACCESS Check for updates

Amino-functionalized magnetic nanoparticles for CO_2 capture

Emanuele Oddo, Ruggiero M. Pesce, Marco Derudi and Luca Magagnin

Department of Chemistry, Materials and Chemical Engineering "G. Natta", Milano, Italy

ABSTRACT

CO_2 accumulation is inducing an effect of global warming. Adsorption using solid sorbents is proving as an effective strategy for CO_2 capture and reuse. The aim of this study was to develop amino-functionalized magnetic nanoparticles by depositing various amines through co-precipitation or impregnation-sonication. Structural characteristics were studied through SEM, BET and XRD analyses, evidencing coarse particles with low crystallinity and surface areas of 100–150 $m^2\ g^{-1}$, while FT-IR confirmed CO_2 interacting with substrate. The load of functional group, particles stability, and CO_2 sorption capacity were assessed through elemental and thermogravimetric analysis. It was found that loads of functional groups ranging from 1.6 to 6.1 wt.%. were deposited, and most samples showed sound stability up to 100°C. Sorption capacities were in the range 0.2–1.5 g g_{NH2}^{-1}, the highest being 1.46 g g_{NH2}^{-1} for ε-aminocaproic acid. Such sample also exhibited good recyclability, with a performance drop of 11% after many cycles. CO_2 uptake decreased with increasing temperature in the range 25–45°C, suggesting a chemical bond between CO_2 and amines. Amino functionalized particles could thus be an interesting solution for CO_2 capture and utilization thanks to fast kinetics, recyclability, and ease of separation.

ARTICLE HISTORY
Received 27 May 2021
Accepted 26 September 2021

KEYWORDS
Adsorption; carbon dioxide; CO_2 activation; amino-functionalization; magnetic nanoparticles

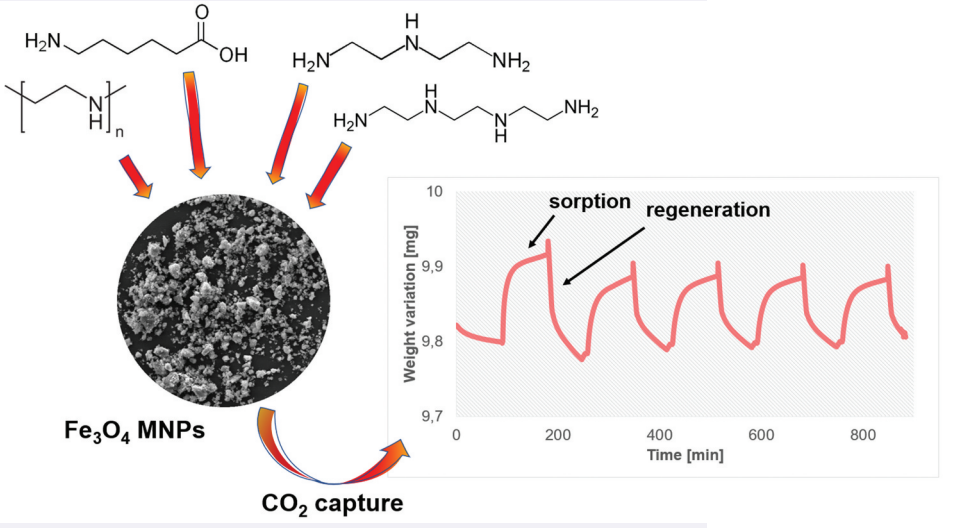

CONTACT Luca Magagnin luca.magagnin@polimi.it Department of Chemistry, Materials and Chemical Engineering "G. Natta", Milano, Italy

© 2021 The Author(s). Published by Informa UK Limited, trading as Taylor & Francis Group.
This is an Open Access article distributed under the terms of the Creative Commons Attribution License (http://creativecommons.org/licenses/by/4.0/), which permits unrestricted use, distribution, and reproduction in any medium, provided the original work is properly cited.

Introduction

Carbon dioxide (CO_2) is a primary greenhouse gas, which provides the thermoregulation of Earth's atmosphere. Since the Second Industrial Revolution, the anthropogenic production of the gas has firmly pushed its accumulation in the atmosphere, inducing an effect of global warming of the atmosphere itself. In fact, the rise in global CO_2 concentration since 2000 has been about 20 ppm per decade, which is up to 10 times faster than any sustained rise in CO_2 during the past 800,000 years [1]. In 2017, atmospheric CO_2 reached 146% of the pre-industrial level of 278 ppm [2]. Also, the excess of atmospheric CO_2 leads to a net air-to-sea flux of excess CO_2. Such a process, known as ocean acidification, leads to predictable changes in the biogeochemical cycles of many elements and the chemistry of seawater [3]. Indeed, the pH of ocean surface water has decreased by 0.1 since the beginning of the industrial era [1]. As such, the need to reduce anthropogenic emissions of carbon dioxide has pushed the development of a broad spectrum of technological-based approaches for emissions mitigation as well as carbon capture, utilization, and storage. However, conventional capture technologies may increase plant energy requirements by 25–40% [4]. Hence, significant efforts have been made in recent years to develop new approaches to improve CO_2 sorption and separation, including separation with polymeric and ceramic membranes [5,6], adsorption, or absorption on different substrates [7–10], or cryogenic-based technologies [11]. In particular, CO_2 adsorption on solid sorbents could be an attractive alternative to the current absorption technologies due to its low-energy requirement [12]. Indeed, CO_2 capture by amine scrubbing is a traditional, widely accepted technology. Still, the regeneration and desorption of CO_2 are energy-intensive due to the high heat of sorption of CO_2 and high regeneration temperature, adding significant operating costs to the capture process [13]. Other drawbacks of such processes include the corrosive nature of the solvents, the accumulation of stable solvent by-products [14], and the generation of products, such as nitrosamine, nitramines and amides, which can affect health and pose environmental risks [13]. On the other hand, solid sorbents are generally characterized by fast adsorption and desorption kinetics, low-energy consumption, simple usage operations, and low-energy demand for their regeneration [15]. Being low adsorption capacity one of the main drawbacks of the process, especially at low partial pressure or in the presence of moisture [14], many substrates (carbonaceous, silica, metal oxides) are functionalized with weakly or covalently bonded small or polymeric amines [13,16–19].

Fe_3O_4 magnetic nanoparticles (MNPs) have recently experienced great popularity due to their unique chemical and physical characteristics. The ferromagnetism allows easy collection and separation of this material, which can be easily obtained in fine powders, even at the nanoscale. Such ease of magnetic separation, combined with the material biocompatibility, have strongly pushed their application in different fields like catalysis and biotechnologies [20–26]. In addition, Fe_3O_4 MNPs have also been effectively exploited for oil and metal ions recovery [27–31], separation of organics in water samples [32] as well as volatile organics and aromatics removal [33–35]. Finally, the possibility of exploit ferromagnetic nanoparticles as solid sorbents for carbon dioxide capture have been explored in few studies in the literature. Liu et al. [36] realized a nanocomposite material by grafting silane-modified polyethyleneimine (PEI, M_w = 400

or 10,000) onto Fe_3O_4 nanoparticles and tested it by dispersing into water at 40°C and 100 kPa, to evaluate CO_2 sorption capacity. The functionalized MNPs were able to effectively capture CO_2 with capacity of 0.373 mol L^{-1} and displayed sound stability over regeneration cycles. Moreover, Li et al. [37] tested magnetite nanoparticles functionalized with various amine polymers. The obtained results clearly highlighted the enhancement of CO_2 capture due to PEI coating as well as the superior CO_2 sorption capacity of PEI compared to all other polymers. In fact, the authors reported CO_2 capacity of 0.34 mmol g^{-1} for 16% PEI (branched, M_w = 25,000) MNPs, paired with good thermal stability and excellent regenerative ability. Even though CO_2 capture through magnetic nanoparticles is hardly found in the literature, it is an intriguing route for several reasons. Fe_3O_4 particles are readily and cost-effectively produced, and they are biocompatible, thus increasing the range of application and reducing the risks connected to their deployment in industrial practice. In addition to this, they display fair thermal stability and selectivity during gas exposure and regeneration, as already highlighted by Li et al. [37], which suggests a high degree of recyclability of the material. Moreover, the ease of separation can be exploited to readily recover the CO_2-loaded particles with little effort. In principle, this could be easily achieved also when particles are exposed to CO_2 within aqueous streams, as their magnetic separation from water is rather simple [38]. For all these reasons, usage of amino-functionalized MNPs could be an interesting approach for carbon capture, utilization, and storage.

Hence, the aim of this study has been to develop different synthesis routes for the production of MNPs coated with several amino groups. The effectiveness of each synthesis pathway has been assessed in terms of resulting coating loaded onto the nanoparticles. All samples were then tested to assess their thermal stability and compare the resulting CO_2 capture capacity, selectivity, and regenerative ability. Furthermore, additional tests were conducted with a reference sample to highlight the impact of operating temperature on the obtained CO_2 uptake. In this way, a general characterization of MNPs performance and a preliminary assessment of their applicability to carbon capture processes could be provided.

Materials and methods

Materials

$FeCl_2$, $FeCl_3$, NaOH, ε-aminocaproic acid, linear polyethyleneimine (LPEI, M_w = 1,200), diethylenetriamine (DETA), triethylenetetramine (TETA), and ethanol were purchased from Sigma-Aldrich.

Preparation of raw and functionalized MNPs

Raw MNPs were prepared by contacting a solution containing a certain amount of Fe^{2+} and Fe^{3+} with a known quantity of a base (NaOH) at room temperature through a pump-siring system. The resulting dispersion is stirred continuously for 30 min. Functionalized MNPs are prepared through two different syntheses, namely co-precipitation and impregnation-sonication. In the first case, the functional group is directly dissolved into the

aqueous solution containing NaOH and the basic solution is contacted with the iron chlorides as described above. In the case of DETA and TETA, few milliliters of ethanol were added to allow complete dissolution of the functional group. Conversely, the impregnation-sonication process is similar to the one described by Li et al. [37]. A certain amount of functional group is dissolved in 25 mL of ethanol and then slowly added under stirring to the MNPs suspended in 25 mL of ethanol. The dispersion is then probe sonicated for 30 min with an ultrasonic homogenizer (UP200St, Hielscher, 50 W). The obtained MNPs were then centrifuged at 5000 rpm several times to allow neutralization of the solution and removal of the dissolved salts (i.e. NaCl). Both synthesis pathways yielded 5 g of either raw or functionalized MNPs. Finally, the samples were dried either at 40°C under vacuum or in a freeze-drier (Telstar LyoQuest Model 61,644, −55°C) for at least 24 h. Particles dried at 40°C experienced agglomeration and were thus grounded to fine powder with mortar and pestle before materials characterization.

Characterization of raw and functionalized MNPs

The obtained samples were characterized by means of thermogravimetric analysis with differential thermal analysis (TGA/DTA) to assess the thermal stability of the different functionalized MNPs using a SDT-Q600 (TA Instruments Inc., USA) apparatus. About 10 mg of each sample were analyzed in the temperature range 30–500°C, always with a heating rate of 1°C/min up to 200°C and then 10°C/min up to 500°C. Nitrogen was used as carrier gas (flow rate of 100 mL/min). TGA/DTA was also exploited to evaluate the CO_2 adsorption capacity and recyclability of all samples through a temperature swing method. Firstly, about 10 mg of each sample were analyzed at 35°C under pure CO_2 flow (flow rate 100 mL/min) for 60 min. In this way, the sorption capacity of functionalized MNPs without any pre-treating was assessed. Then, the samples were heated up to 100°C with a heating rate of 10°C/min under inert flow (i.e. Nitrogen) and kept constant for 120 min. Then, the conditioned sample was cooled back to 35°C and exposed to the pure CO_2 flow as for the previous step (flowrate 100 mL/min). This cycle was repeated four times. In addition, cycles of sorption/regeneration at different sorption temperatures, namely 25 and 45°C, were carried out to assess the influence of temperature on the resulting CO_2 capture. Selectivity studies were also carried out, basically in the same condition as conventional sorption, by flushing at 35°C pure Oxygen, Nitrogen or methane in the place of CO_2 (flow rate 100 mL/min).

Moreover, about 5–10 mg of the obtained samples were characterized by means of CHNS elemental analysis to assess the actual load of functional groups. CHNS was preferred to TGA/DTA for this purpose in order to avoid overestimation of the coating load due to residual humidity in the sample. The Carbon content obtained from CHNS analysis was exploited along with the Carbon fraction in the functional group to derive the coating load according to Equation (1):

$$Coating = f_C/\omega_C = f_N/\omega_N \tag{1}$$

Where the coating is defined either as [mg] or [wt.%], f_C is the Carbon content in the sample in [mg] or [wt.%] and ω_C is the Carbon fraction in the functional group [g/g]. As shown in the equation, the actual load can also be derived from the Nitrogen content f_N (in [mg] or [wt.%]) and the Nitrogen fraction ω_N [g/g] in the same way. Raw and functionalized particles were also characterized using a scanning electron microscope

(SEM) operated at 20 kV. Brunauer-Emmett-Teller (BET) surface area was evaluated through measurements of N_2 adsorption/desorption isotherm with a TriStar 3000 instrument (Micromeritics). The corresponding surface area was retrieved with BET multipoint method. Total pore volume and average pore size were retrieved according to the BJH method. Solid-state Fourier transform infrared spectra (FT-IR) were obtained on a iS50 FTIR Spectrometer (Thermo Scientific Nicolet). The analysis was performed through attenuated total reflection (ATR) technique and the spectra were collected between 400 to 4000 cm^{-1}. FT-IR measures were carried out before and after CO_2 exposure to investigate carbon dioxide interaction with substrates. X-ray diffraction (XRD) measures were performed on functionalized MNPs at room temperature from 20 to 80 2θ degree. XRD tests were carried out using a Bruker D8 Advance, equipped with a Cu Ka X-ray source at 40 kV and 40 mA.

Results and discussion

MNPs samples were functionalized with four different functional groups: ε-aminocaproic acid (ε-MNPs), linear polyethyleneimine (PEI-MNPs), diethylenetriamine (DETA-MNPs), and triethylenetetramine (TETA-MNPs). Functional groups were selected to provide a good variety of MNPs coating, including amino acid, amines, and a polymer.

A preliminary screening was carried out to assess the optimal synthesis path for amine and amino acid functional groups. Thus, MNPs samples were prepared by dissolving in the synthesis solution 2 g of functional group for both ε-aminocaproic acid and linear PEI through both co-precipitation and impregnation-sonication pathways. The resulting particles were then studied using CHNS elemental analysis to assess the corresponding actual load of functional group onto the particle surface. Each sample was analyzed in three replicates, with sample weight varying in the range 5–10 mg, and the deviation for Carbon and Nitrogen contents was always below 0.1 wt.%.

Figure 1 reports coating loads derived for the ε- and PEI-MNPs samples prepared through the two synthesis pathways. It can be seen that co-deposition (co-dep) provides a higher amount of functional group for the ε-MNPs (2 g of functional group) compared to the impregnation-sonication (imp-son) technique. Aminocaproic acid is grafted onto the surface of the particles through the formation of a strong polar covalent bond. Such a process may be facilitated if the functional group is made available during the MNPs formation, accounting for the higher load obtained with the co-deposition method. Conversely, PEI-MNPs provided a higher load of coating with the impregnation-sonication method. It is reported that amine can be impregnated onto the support through physical adsorption [13]. In addition, PEI may be able to reticulate around the particles, producing a sort of shell and thus increasing the amount of deposited polyamine. These physical processes are probably fostered by the sonication of the MNPs dispersion, resulting in the higher load for the impregnation-sonication case. Furthermore, the coating load as computed from the Carbon fraction was similar to the one derived from the Nitrogen fraction and the corresponding Nitrogen to Carbon ratio was very close to the theoretical value for both aminocaproic acid and PEI. This suggests that apparently no significant alteration of the functional group structure took place during deposition. DETA- and TETA-MNPs yielded comparable coating loads for the two syntheses. As such, co-deposition was preferred for the sake of simplicity.

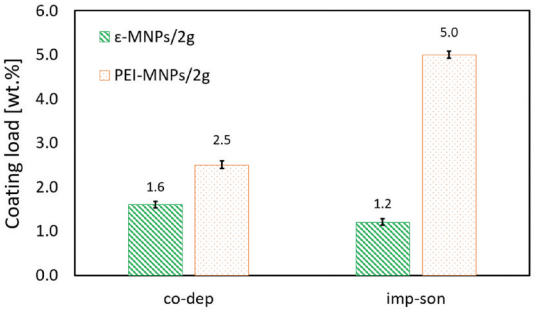

Figure 1. Coating load of preliminary sample of ε-MNPs and PEI-MNPs (2 g of functional group), according to the two synthesis pathways.

Another screening was performed to assess the impact of the drying methodology on the sorption performances of the particles. Raw MNPs and functionalized ε- and PEI-MNPs were prepared dissolving 2 g of functional group in solution and were alternatively dried at 40°C under low vacuum or freeze-dried. Along with functionalized samples, raw particles were also tested in this phase to highlight the effects of drying methods both on the substrate structure (e.g. reduced surface area and porosity) and the functional groups. The ability of MNPs to capture carbon dioxide was evaluated through TGA/DTA analysis, by exposing the particles to a pure CO_2 flow (flow rate of 50 mL/min) for 180 min at 35°C, and the sorption capacity was computed as mg of captured carbon dioxide per gram of particles. The resulting capacities are reported in Figure 2 for all preliminary samples. CO_2 uptake is expressed as mg of captured CO_2 per gram of particles, differently from the following sections of the study where all sorption capacities are expressed in terms of g of captured CO2 per gram of loaded functional group. In fact, expressing the CO_2 uptake as $mg_{CO2}\ g_{MNP}^{-1}$ was more convenient for comparison with pristine particles.

Sample of ε-MNPs displayed a significant drop in sorption capacity after drying in the oven, which was reduced roughly by a factor of two with respect to the freeze-dried sample. This could be explained considering that all MNPs samples experienced substantial aggregation after conventional drying and required grinding with mortar and pestle. Firstly, grinding process undoubtedly results in higher granulometry compared to freeze-dried samples, providing lower surface area available for CO_2 sorption. Furthermore, grinding of the particles may also mechanically damage the functional group, reducing the availability of amino groups for carbon dioxide chemical adsorption. By contrast, PEI-MNPs exhibited very similar sorption capacities for the two drying methods, with a slightly higher value for conventional drying. This may be due to the tendency of PEI to reticulate around the particle, which may have increased its mechanical resistance to the grinding process. Finally, raw MNPs proved themselves able to effectively capture CO_2, with sorption capacity comparable to functionalized particles, at least after freeze-drying. It should be stressed, though, that in this case CO_2 is captured through physical absorption instead of chemical adsorption. Thus it is not expected to be stable and selective as for functionalized samples. Moreover, raw MNPs experienced a dramatic decrease in the sorption capacity by changing the drying method. Carbon uptake was reduced by a factor of three with

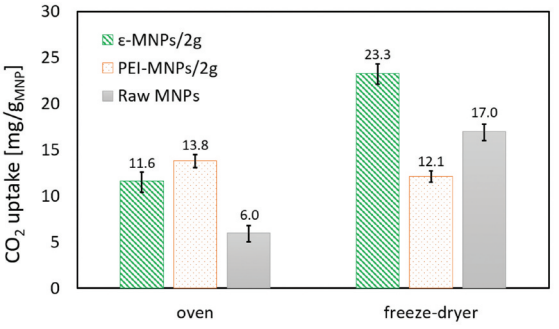

Figure 2. Sorption capacity of preliminary samples of raw particles and functionalized ε-MNPs and PEI-MNPs (2 g of functional group), according to the two drying methodologies.

conventional drying with respect to the freeze-dried sample – a performance drop even higher than in the case of ε-MNPs. Such behavior confirms that conventional drying is strongly affecting the whole particle rather than the amino group alone.

According to these preliminary results, following samples have been prepared selecting the optimal synthesis pathway for each group, namely co-deposition for aminocaproic acid, DETA and TETA and impregnation-sonication for PEI. Also, freeze-drying was selected as the only drying methodology for all remaining samples to avoid any issue related to particles agglomeration and damaging functional groups. In the following tests, MNPs were functionalized with each group using three amounts of functional group (1, 1.5 and 2 g), for a grand total of 12 samples. At the end of the synthesis, all specimens appeared as black, fine powder and they retained magnetic properties despite being coated with functional groups.

Firstly, samples were characterized by means of CHNS elemental analysis to assess the actual load of each functional group deposited on the particles surface. Such analysis is essential to properly pair MNPs performances to the actual load of coating rather than the nominal weight of functional group. In principle, TGA/DTA could be exploited to the same end by evaluating the weight variation due to functional group degradation at high temperature. However, results from such analysis were not reliable due to residual humidity embedded in the core of the particles, which may have led to overestimating the amount of coating deposited onto the particles. For this reason, CHNS was preferred for the evaluation of functional group load. The resulting coating loads for all tested samples, as computed from Equation (1), are shown in Figure 3.

Firstly, it is evident that all amino functional groups were successfully deposited onto the particles surface. However, all samples provided lower amounts of coating compared to the nominal weight. Indeed, the ratio between group load and nominal weight varies in the range 0.04–0.24, with the highest for PEI-MNPs/1 g and the lowest for ε-MNPs/2 g. ε-MNPs displayed almost the same coating load for all analyzed samples. Apparently, the available sites for grafting the amino acid are quickly saturated, even at the lowest nominal weight, and the further addition of functional group has no impact on the deposited coating. As the coating load is pretty small (1.6 wt.%), it is reasonable to assume

that aminocaproic acid covers the particles with a single tiny layer, tied to the surface with a strong polar covalent bond. On the other hand, DETA- and TETA-MNPs exhibited higher coating load with respect to ε-MNPs, varying between 2.0 and 6.1 wt.%.

Interestingly, both functional groups did not report the highest amount using 2 g of functional group, as one would expect, but at 1.5 g. This unusual trend could be due to the high concentration of functional group in solution when dissolving 2 g, which may have hindered the contacting between particles and the amino group. Indeed, the coating load of TETA-MNPs/2 g is even lower than the one obtained with 1 g. Lastly, PEI-MNPs showed roughly the same amount of coating for all nominal weights, similarly to ε-MNPs samples. This could be explained given the ability of PEI to reticulate, producing a sort of shell around the particles. Such shell may cover the active sites for the impregnation, thus preventing the deposition of additional coating at higher amounts of functional group.

SEM images of pristine MNPs are shown in Figure 4. Particles are clearly agglomerated with variable size and shape (Figure 4A), with the largest clusters in the range of tens of μm (Figure 4B). Comparison between raw and functionalized MNPs revealed no significant change in the particles agglomeration due to ammine grafting.

Results from FT-IR analysis of raw and functionalized MNPs before CO_2 exposure are reported in Figure 5. Pristine nanoparticles display a sharp peak near 500 cm^{-1}, which was assigned to Fe-O-Fe stretching vibration (Figure 5A). Also, some peaks due to residual water were highlighted in the region 3500–3100 cm^{-1} as well as two peaks near 1600 and 1300 cm^{-1}. Compared with raw MNPs, functionalized samples showed an additional peak around 1600 cm^{-1}, which was attributed to N-H bending, and a shoulder around 1400 cm^{-1}, probably due to C-H bending vibrations (Figure 5B). Moreover, ε- and PEI-MNPs evidenced two peaks in the 3000–2800 cm^{-1} region, which were ascribed to C-H stretching vibrations. Along with CHNS analysis, FT-IR spectra confirmed that the functional groups were effectively deposited onto the surface of the particles.

The Brunauer-Emmett-Teller (BET) method was used to evaluate the specific surface area of particles reported in Table 1 for pristine and functionalized MNPs. Raw MNPs provided a specific area of 96 $m^2\ g^{-1}$, while the deposition of the functional group surprisingly raised the specific surface area of MNPs of about 35–55 $m^2\ g^{-1}$. This may be due to the functional group preventing or at least partially hindering agglomeration phenomena, which arise during drying. This is coherent with the sorption capacity of pristine MNPs dropping much more than functionalized ones when switching from

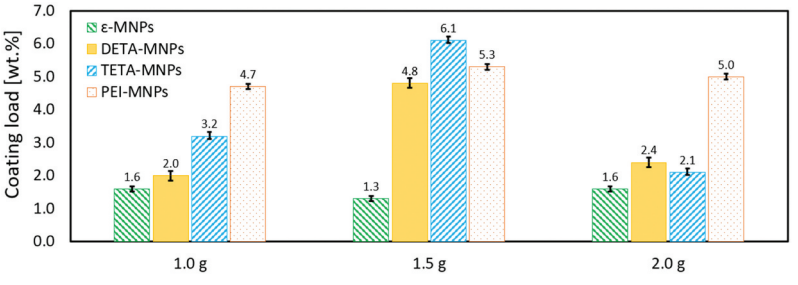

Figure 3. Coating load of functionalized MNPs for different amounts of functional group in solution, as retrieved from elemental CHNS analysis.

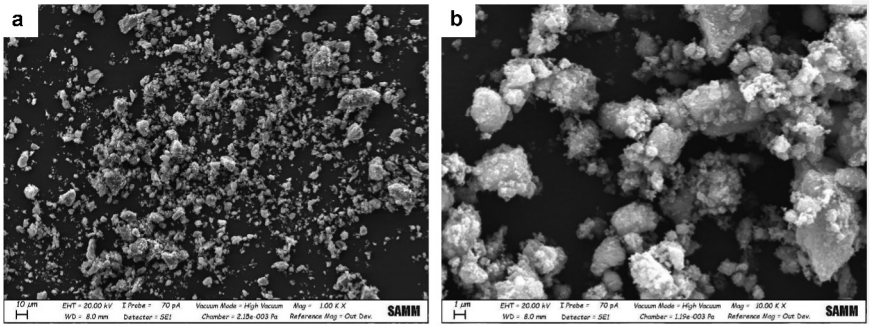

Figure 4. SEM images of pristine magnetic nanoparticles.

lyophilization to conventional drying. An exception to this trend is PEI-MNPs, which yielded a surface area slightly lower than the pristine samples. But it is not surprising as PEI is expected to reticulate around the particles, thus covering part of the pores.

Figure 6 reports the diffraction patterns for ε-MNPs/2 g sample. Diffraction peaks were identified at 18.4°, 30.2°, 35.4°, 42.4°, 53.2°, 56.9° and 62.4°, which are ascribed to ICSD 98–015-8741 (iron oxide as magnetite with low crystallinity). The pattern is very similar to the one obtained for pristine particles, suggesting that the general structure and crystallinity of the particle aggregates are not affected by the amine deposition. This is true also for the other functional groups, as very similar diffraction patterns were retrieved, always in good agreement with the ICSD reference.

Lastly, all functionalized specimens retained magnetic properties after coating deposition. As shown in Figure 7, particles were easily attracted to a weak laboratory magnet. In addition, they could be easily separated from water after dispersion, still with the aid of a small magnet.

MNPs were then tested through TGA/DTA to assess their thermal stability in the range 30–500°C. All samples highlighted a variable weight loss below 100°C, accounting for 2.5–5 wt.% of the total weight, depending on the sample. This moderate weight loss is essentially due to the removal of residual water physically absorbed onto the surface of the particles as well as water embedded in the particle pores. Indeed, such weight loss is still higher than the coating load deposited onto some samples, namely all ε-MNPs specimens. Still, all samples displayed sound stability up to 100°C. So long as sufficient time is provided at low temperature for water removal, no other significant weight loss was detected below 100°C. The TGA/DTA plot for the thermal analysis of ε-MNPs/2 g is reported as an example in Figure 8.

As the degradation of some functional group (notably DETA) starts just above 100°C, such temperature was defined as the boundary temperature for regeneration of particles after CO_2 capture.

Next, the sorption capacity of 2 g samples was evaluated through TGA/DTA tests, in terms of grams of CO_2 captured per gram of loaded functional group. Differently from preliminary screening, sorption capacities expressed as $g_{CO2}\ g_{NH2}{}^{-1}$ were preferred for all subsequent experiments to better highlight the actual exploitation of the functional group. The regenerative ability of all tested samples was assessed using a temperature swing method. The cycle of exposure to pure CO_2 and consequent regeneration in inert

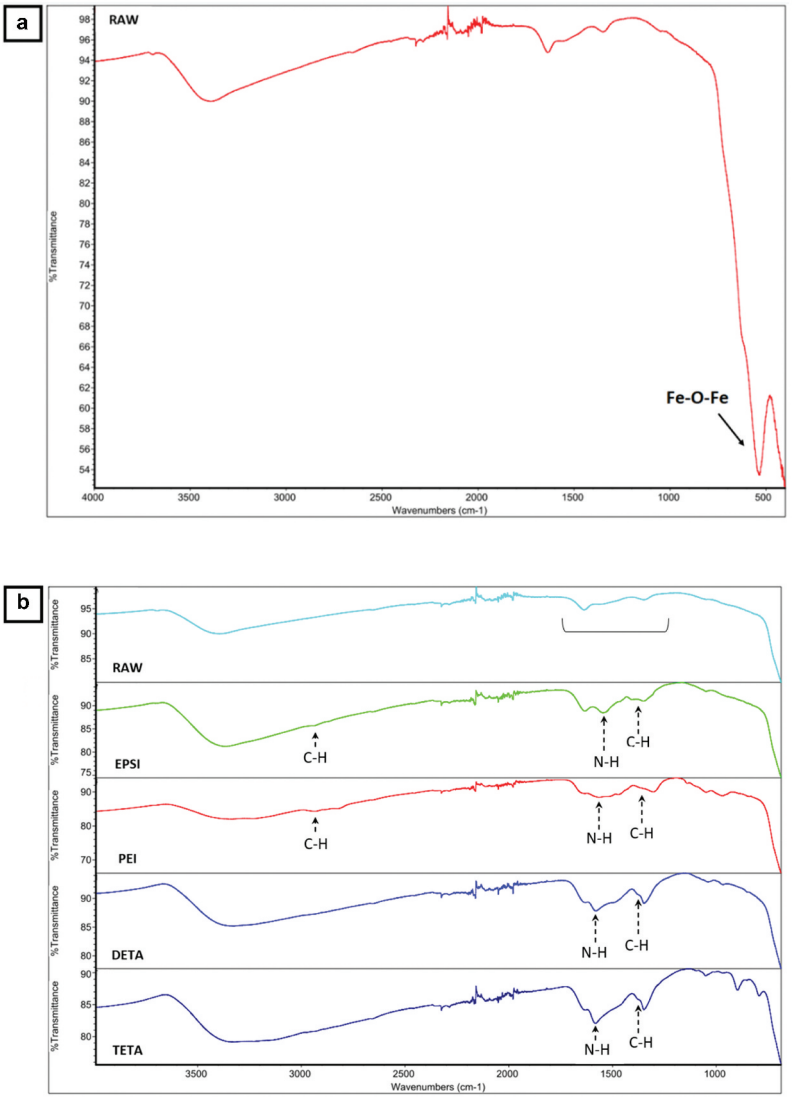

Figure 5. FT-IR spectra of pristine MNPs (A) and comparative spectra of raw and functionalized MNPs with all four functional groups (B).

Table 1. Specific surface area ($m^2\ g^{-1}$), total pore volume ($cm^3\ g^{-1}$) and average pore size (nm) of pristine and functionalized MNPs.

Sample	Surface area	Total pore volume	Average pore size
Pristine MNPs	96.2	0.284	10.1
ε-MNPs/2 g	152.2	0.257	5.9
DETA-MNPs/2 g	147.0	0.141	4.8
TETA-MNPs/2 g	131.6	0.174	5.2
PEI-MNPs/2 g	95.7	0.279	10.0

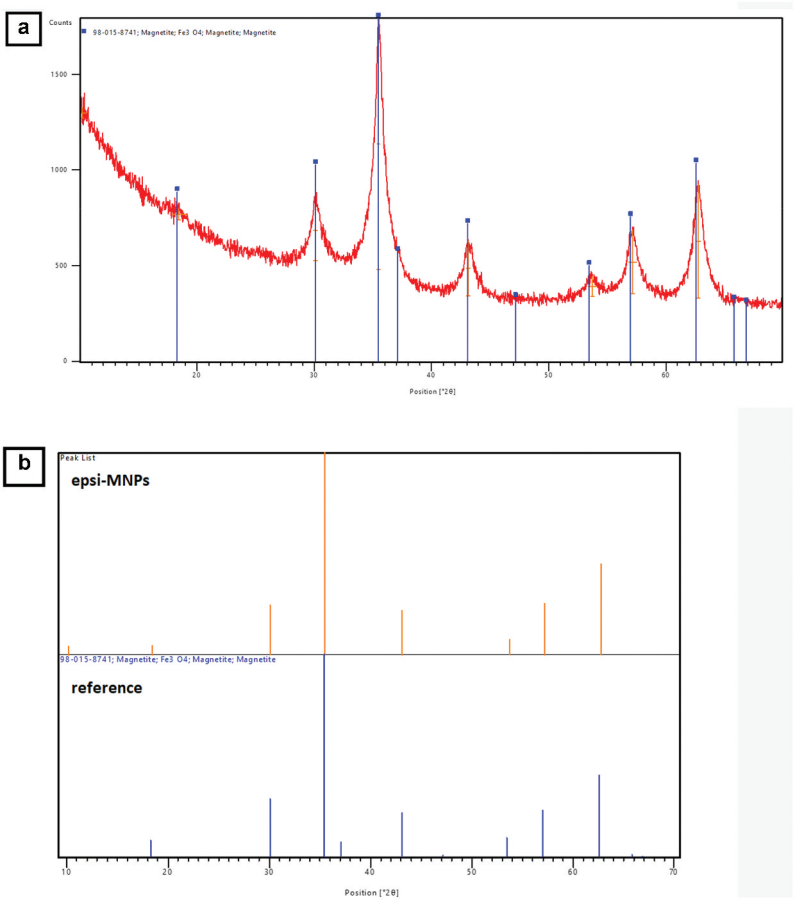

Figure 6. XRD measurements on ε-MNPs/2 g sample (A) and comparison with Fe_3O_4 reference XRD spectra (B).

Figure 7. ε-MNPs interaction with a small laboratory magnet.

atmosphere was repeated at least four times for all samples, so that the stability of specimens after repeated utilization could be examined. Moreover, an additional sorption test was performed before these four cycles, to assess the particles performance without

any conditioning (i.e. drying/regeneration at high temperature). As an example, Figure 9 shows the TGA plot of 1.6 wt.% ε-MNPs for the five (one raw plus four conditioned) capture-regeneration cycles.

It can be seen that CO_2 capture during the first exposure was very fast, with nearly 90% of the total CO_2 uptake collected in 15 min. In addition, it is evident that the sample is effectively regenerated at 100°C, as the weight loss due to regeneration is generally consistent with the weight increase during exposure to carbon dioxide. After regeneration, the sample can still effectively capture carbon dioxide, but the sorption capacity is reduced and the required time for complete collection is sharply increased, as more than 60 min are needed to approach the asymptotic value. Such behavior is common to all tested samples and suggests an alteration of MNPs surface after regeneration. Nonetheless, the following capture-regeneration curves are very similar to one another, with minor decrease in the sorption capacity of the sample between the cycles.

Sorption capacities at the first conditioned cycle (i.e. first cycle after heating to 100°C) for all functional groups are synthesized in Figure 10. Most samples displayed sorption capacities of 1–1.5 g per gram of functional group (g_{NH2}), confirming their ability to capture CO_2 effectively. Despite having the lowest coating load, ε-MNPs stands out with the highest capacity among all tested samples, corresponding to 1.46 g g_{NH2}^{-1}. The 2.4 wt.% DETA-MNPs sample showed good sorption capacity as well, close to ε-MNP and almost twice the capacity of raw particles. This is consistent with the measured surface area, almost as high as ε-MNPs. Unfortunately, such sample also experienced a continuous decrease of performance (i.e. sorption capacity) cycle upon cycle, as discussed later in this study. Conversely, 5 wt.% PEI-MNPs exhibited a poor sorption capacity of just 0.24 g g_{NH2}^{-1}, which is even lower than the capacity of pristine MNPs. This is undoubtedly also due to the low surface area of PEI-MNPs, which was found to be even lower than that of raw particles. Still, it should be stressed that raw MNPs can only capture CO_2 through weak physical absorption, resulting in lower selectivity and stability compared to functionalized sorbents, however poor their sorption capacity may be. Furthermore, the obtained capacity for 5 wt.% PEI-MNPs (12.1 mg g_{MNP}^{-1}) is roughly 80% of the one reported by Li et al. [37] for 16% PEI (branched, M_w = 25,000) MNPs, namely 15.0 mg g^{-1}. This is

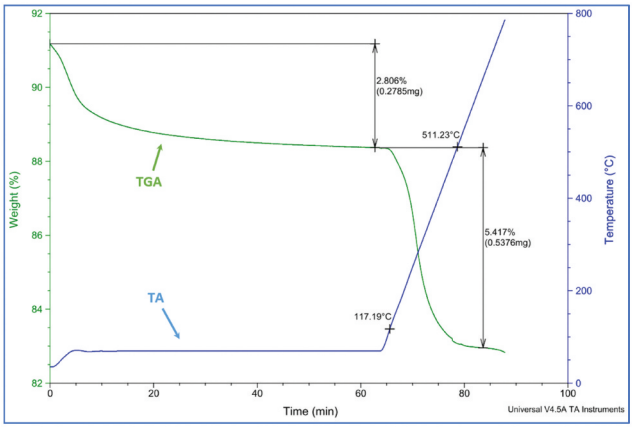

Figure 8. TGA results of the thermal analysis of ε-MNPs/2 g sample.

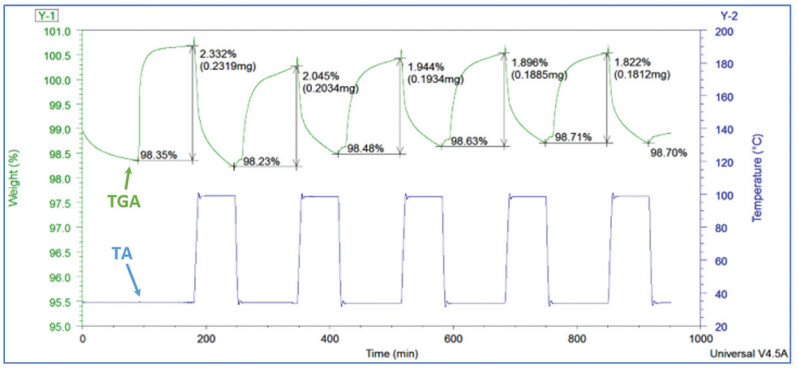

Figure 9. TGA plot of 1.6 wt.% ε-MNPs sample during CO_2 sorption and regeneration cycles.

remarkable considering the limited molecular weight of the polymer used in this study (M_w = 1,200), since Li et al. [37] reported increasing sorption capacity (and specific surface area) with increasing molecular weight of the polymer. In this respect, a comparison between the sorption capacities of the present study and those obtained by Li et al. [37] is proposed in Table 2. It is shown how the sorption capacities are generally greater (at least one order of magnitude) than those reported by Li et al. [37] for PEI-decorated particles. As a side note, the sorption capacity reported by Liu et al. [36] was not included in this selection as it was retrieved in rather different conditions (high pressure and aqueous medium).

As a more general remark, the sorption capacities of this work are typically lower than that of other, more common substrates, as for example zeolites or activated carbon [4,19], but the ease of separation of MNPs could be beneficial for the subsequent reuse of captured CO_2. For instance, should CO_2 utilization take place in the liquid phase (e.g. electrochemical conversion), particles recovery after CO_2 release would greatly benefit from their magnetic properties.

The selectivity of the sorption was evaluated with respect to three key species, namely Oxygen, Nitrogen, and methane. The latter is particularly relevant as it may be found in significant amounts in exhaust gases from many industrial processes. Figure 11 reports

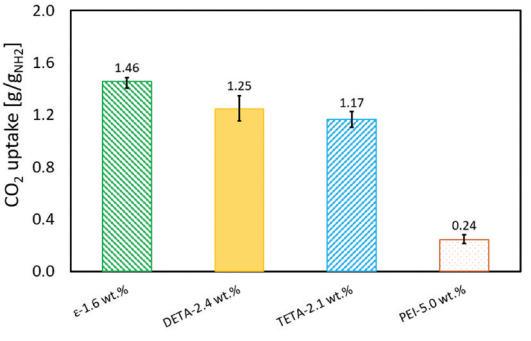

Figure 10. Sorption capacities at the first conditioned cycle of functionalized MNPs as retrieved from TGA/DTA analysis.

the selectivity of CO_2 over Oxygen, Nitrogen, and methane for 1.6 wt.% ε-MNPs sample. It is evident how the carbon dioxide uptake is dramatically higher compared to that of methane, which was estimated as 0.013 g/g_{NH2}. As for O_2 and N_2, the variation was even slightly negative (i.e. weight loss), which was attributed to the loss of some residual humidity stripped by the gas flow. As such, a high selectivity of CO_2 over other species was demonstrated. Comparable results were also retrieved by TGA/DTA of the other specimens: Oxygen and Nitrogen streams always yielded negative weight variation, while CH_4 sorption capacities were 0.038, 0.009 and 0.034 g g_{NH2}^{-1} respectively for DETA-, TETA- and PEI-MNPs, at least two orders of magnitude below the CO_2 sorption capacity (except for PEI, which was still one order below). These results are relevant for assessing the applicability of the material for CO_2 capture in real-world streams, but further studies involving more complex mixtures (e.g. containing H_2S) would certainly be desirable.

As already mentioned, the kinetics of adsorption slowed down significantly after the first cycle, requiring at least 40 min, depending on the type of coating, to approach the asymptotic CO_2 uptake. This is probably due to some change in the surface morphology of tested MNPs, altering the availability of sites for adsorption. Still, the shape of the capture-regeneration curve after first regeneration is essentially unaffected for subsequent cycles, with the only exception of DETA-MNPs. Such sample displayed significant losses in sorption performances after each regeneration, suggesting that the functional group was progressively degraded at high temperature. This is reasonable, considering that thermal analysis of DETA evidenced degradation barely above 100°C. Hence, such particles underwent an additional heating program, where regeneration was performed at milder conditions (70°C) to prevent DETA degradation. However, the decrease in the regeneration temperature led to a dramatic increase in the time required for CO_2 release. 120 min were not enough to completely restore MNPs to their original weight. This resulted in lower CO_2 uptake and an even higher performance drop, with sorption capacity drop of 34% just after one cycle.

Figure 12 reports the computed performance drop at the second (conditioned) cycle, at the third cycle, and after four cycles. The dramatic loss in performance is evident for DETA-MNPs, with 30% decrease after just one cycle. Indeed, the drop at the end of all cycles was not reported for the sake of graph readability, as it easily exceeds 50%. ε-MNPs slightly decreased CO_2 uptake between one cycle and the other, but the overall performance drop was slightly above 10%, confirming that such specimen is fairly stable even at regeneration temperature. Similarly, TETA-MNPs experienced a major drop at the first

Table 2. Comparison between sorption capacities (as g g_{NH2}^{-1}) obtained in this work and those of reported by Li et al. (2017) [37].

Sample	CO_2 uptake	Reference
ε (1.6 wt.%)	1.46	This work
DETA (2.4 wt.%)	1.17	This work
TETA (2.1 wt.%)	1.25	This work
PEI (linear, M_w = 1,200, 5 wt.%)	0.24	This work
PEI (branched, M_w = 1,800, 16 wt.%)	0.088	Li et al. (2017) [37]
PEI (branched, M_w = 10,000, 16 wt.%)	0.091	Li et al. (2017) [37]
PEI (branched, M_w = 25,000, 16 wt.%)	0.094	Li et al. (2017) [37]
PEI (linear, M_w = 25,000, 16 wt.%)	0.103	Li et al. (2017) [37]

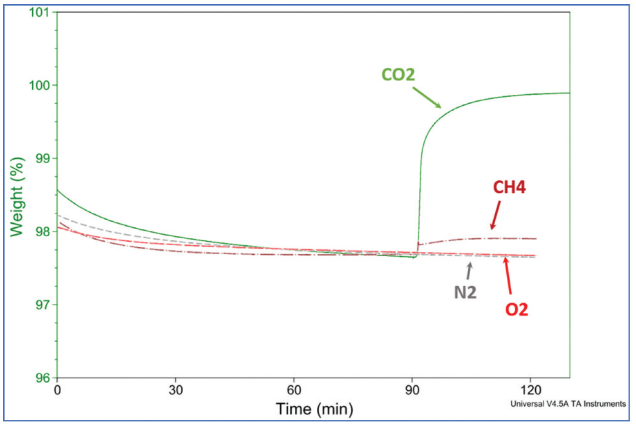

Figure 11. TGA plot of 1.6 wt.% ε-MNPs sample during CO_2, O_2, N_2 and CH_4 exposure.

cycle, close to 20%, but then the sorption capacity was more stable. On the other hand, PEI-MNPs showed a monotonic decrease of sorption capacity, which subtly slowed down at the fourth cycle.

Amino functional groups are expected to interact with carbon dioxide *via* the formation of chemical bonds. Notably, primary and secondary amines may react with CO_2 to form carbamate under dry conditions or bicarbonate at the secondary amine sites in the presence of water [39], according to:

$$RNH_2 + CO_2 \rightarrow RNHCO_2^- + H^+ \tag{2}$$

$$RNH_2 + CO_2 + H_2O \rightarrow RNH_3^+ + HCO_3^- \tag{3}$$

As such, the sorption capacity is expected to increase with decreasing temperature and vice versa due to process exothermicity. Thus, TGA/DTA was also exploited to assess the sorption capacity at different sorption temperatures. Equivalent samples of 1.6 wt.% ε-MNPs were exposed to the CO_2 flux at 25, 35 and 45°C. As a result, it was found that CO_2 uptake decreased monotonically with temperature with capacities of 1.5–1.08 g g_{NH2}^{-1}, as shown in Figure 13.

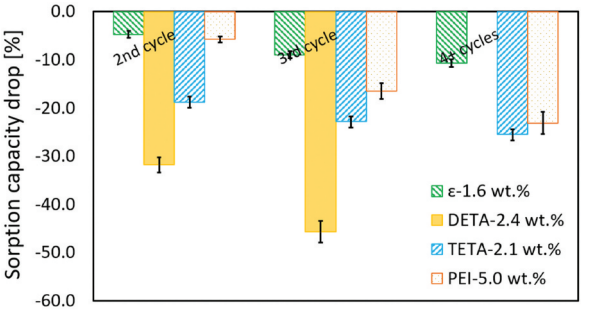

Figure 12. Performance drop in the sorption capacities at 2nd, 3rd and 4+ cycles for all functionalized MNPs as retrieved from TGA/DTA analysis.

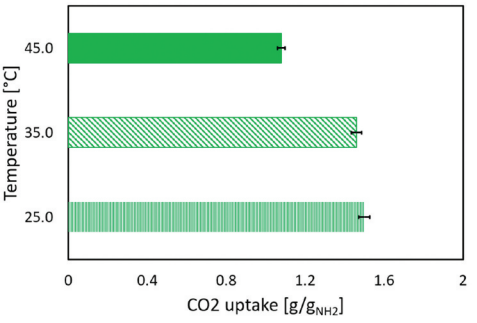

Figure 13. Effect of temperature on CO_2 uptake at the first (conditioned) cycle for 1.6 wt.% ε-MNPs.

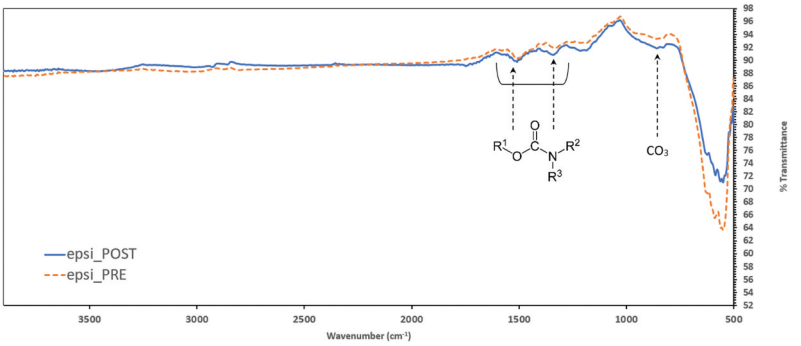

Figure 14. FT-IR spectra of ε-MNPs sample acquired before (dashed line) and after CO_2 exposure (solid line).

These results are consistent with the suggested reaction path leading to the formation of chemical bonds between carbon dioxide and the functional group. Evidently, the lower the sorption temperature the easier the regeneration due to the increased temperature differential, allowing the full release of carbon dioxide in less time. The temperature of 35°C, at which most of the capture experiments were carried out, appears as a reasonable compromise considering the limited increase in CO_2 uptake switching to 25°C.

Further evidence of the formation of carbamates and bicarbonates was provided by FT-IR analysis of MNPs after carbon dioxide exposure. CO_2 sorption gave rise to a series of new peaks which can be attributed to carbonated species. As an example, FT-IR spectra of ε-MNPs after the first conditioned cycle is reported in Figure 14. It can be seen that the shape of the spectra is affected by CO_2 uptake, especially in the region 1600–1300 cm^{-1}. Two new peaks were highlighted at 1510 cm^{-1} and 1340 cm^{-1}, which were ascribed to asymmetric and symmetric stretch of carbamate. Moreover, an additional peak was spotted near 850 cm^{-1}, which can be assigned to carbonate. Similar results were also found for the other functional groups, with FT-IR analysis evidencing carbamate peaks in the range 1600–1300 cm^{-1}. The presence of the peaks was less pronounced in the case of PEI-MNPs, which is probably due to both low sorption capacities of PEI and high coating load (broader peaks of polyamine). On the other hand, the peak of CO_3^{2-} was identified also for that sample.

Conclusions

The aim of this study has been to develop magnetic nanoparticles coated with different amino functional groups, to be used for CO_2 capture and utilization. It was shown that all functional groups were effectively deposited onto the particles surface, although large amounts of each group (1–2 g) resulted in moderate coating loads, in the range of 1.7–6.1 wt.%. SEM analysis of MNPs showed that particles agglomerated in clusters with different shapes and variable sizes, up to tens of microns. Still, all functionalized particles retained magnetic properties and showed sound stability up to 100°C, and most samples also evidenced an increase of specific surface as a result of coating deposition. It was clearly highlighted that effective deposition can be achieved for a wide variety of amines. As the available studies in the literature were focused on amine polymers, the results of the present work widened substantially the list and nature of MNPs functional groups studied for CO_2 capture This is particularly relevant for amino-acids, considering that ε-MNPs displayed the highest sorption capacity and stability.

Sorption tests were performed through TGA/DTA analysis, showing that functionalized MNPs can effectively capture carbon dioxide with sorption capacities of 0.24–1.5 g g_{NH2}^{-1}, depending on the type of functional group, the highest being 1.46 g g_{NH2}^{-1} for 1.6 wt.% ε-MNPs. Several cycles of CO_2 sorption and particles regeneration at high temperature clearly evidenced that ε-MNPs exhibits good recyclability and stability, losing only 11% of sorption capacity after four cycles and approaching a plateau, while DETA-MNPs experienced a drop of more than 30% after just one cycle, suggesting that the functional group was irreversibly degraded during regeneration. Finally, the effect of temperature on sorption capacity was assessed in the range 25–45°C, revealing that the higher the temperature the lower the corresponding CO_2 uptake. This result is consistent with the hypothesis of an exothermic reaction between CO_2 and the amino groups, leading to the formation of carbamates or bicarbonates.

The obtained results showed higher sorption capacities with respect to other reported in the literature for amino-functionalized MNPs and sound stability and recyclability. Such ability to readily capture and release CO_2 could set the basis for an easy-scalable process for CO_2 capture and utilization. This is even more true considering alternative application in the liquid phase, where the ease of magnetic separation could be crucial for process profitability. Indeed, the particles' stability, recyclability, fast kinetics, and scalability may remove some obstacles typically encountered when dealing with CO2 capture and reuse processes at the industrial level.

Disclosure statement

The authors declare that they have no known competing financial interests or personal relationships that could have appeared to influence the work reported in this paper.

Funding

This research did not receive any specific grant from funding agencies in the public, commercial, or not-for-profit sectors.

ORCID

Luca Magagnin http://orcid.org/0000-0001-5553-6441

References

[1] Masson-Delmotte V, Zhai P, Pörtner HO, et al., Eds. Global warming of 1.5°C: an IPCC Special Report on the impacts of global warming of 1.5°C above pre-industrial levels and related global greenhouse gas emission pathways, in the context of strengthening the global response to the threat of climate change, sustainable development, and efforts to eradicate poverty. Geneva, Switzerland: World Meteorological Organization; 2018.
[2] World Metereological Organization. Bulletin: Realizing the WMO 2030 Vision 68, 2019.
[3] Zeng X, Chen X, Zhuang J, et al. The positive relationship between ocean acidification and pollution. Mar Pollut Bull. 2015;91:14–21.
[4] D'Alessandro DM, Smit B, Long JR, et al. Carbon dioxide capture: prospects for new materials. Angew Chem Int Ed Engl. 2010;49:6058–6082.
[5] Ji G, Zhao M. Membrane Separation Technology in Carbon Capture. In: Yun Y, editor. Recent advances in carbon capture and storage. Croatia: InTech, Rijeka; 2017; 59-84.
[6] Jiang S, Ladewig BP. Green synthesis of polymeric membranes: recent advances and future prospects. Current Opinion in Green and Sustainable Chemistry. 2020;21:1–8.
[7] Ben-Mansour R, Habib MA, Bamidele OE, et al. Carbon capture by physical adsorption: materials, experimental investigations and numerical modeling and simulations – a review. Appl Energy. 2016;161:225–255.
[8] Wang M, Li Y, Pan M, et al. Shape-customizable macro-/microporous Carbon monoliths for structure-to-functionality CO 2 adsorption and novel electrical regeneration. Adv Mater Technol. 2017;2:1700088.
[9] Mukherjee A, Okolie JA, Abdelrasoul A, et al. Review of post-combustion carbon dioxide capture technologies using activated carbon. J Environ Sci (China). 2019;83:46–63.
[10] Ma X, Li L, Chen R, et al. Doping of alkali metals in carbon frameworks for enhancing CO2 capture: a theoretical study. Fuel. 2019;236:942–948.
[11] Song C, Liu Q, Deng S, et al. Cryogenic-based CO2 capture technologies: state-of-the-art developments and current challenges. Renew Sust Energ Rev. 2019;101:265–278.
[12] Sjostrom S, Krutka H. Evaluation of solid sorbents as a retrofit technology for CO2 capture. Fuel. 2010;89(6):1298–1306.
[13] Varghese AM, Karanikolos GN. CO2 capture adsorbents functionalized by amine – bearing polymers: a review. Int J Greenhouse Gas Control. 2020;96:103005.
[14] Chaffee AL, Knowles GP, Liang Z, et al. CO2 capture by adsorption: materials and process development. Int J Greenhouse Gas Control. 2007;1(1):11–18.
[15] Nocito F, Dibenedetto A. Atmospheric CO2 mitigation technologies: carbon capture utilization and storage. Current Opinion in Green and Sustainable Chemistry. 2020;21:34–43.
[16] Chaikittisilp W, Kim H-J, Jones CW, et al. Mesoporous alumina-supported amines as potential steam-stable adsorbents for capturing CO 2 from simulated flue gas and ambient air. Energy Fuels. 2011;25:5528–5537.
[17] Choi S, Drese JH, Jones CW, et al. Adsorbent materials for carbon dioxide capture from large anthropogenic point sources. ChemSusChem. 2009;2(9):796–854.
[18] Abid HR, Shang J, Ang H-M, et al. Amino-functionalized Zr-MOF nanoparticles for adsorption of CO 2 and CH 4. Int J Smart Nano Mater. 2013;4(1):72–82.
[19] Liu C, Xing W, Zhou J, et al. N-containing activated carbons for CO2 capture. Int J Smart Nano Mater. 2013;4(1):55–61.
[20] Nishio K, Ikeda M, Gokon N, et al. Preparation of size-controlled (30–100nm) magnetite nanoparticles for biomedical applications. J Magn Magn Mater. 2007;310(2):2408–2410.

[21] Munoz M, De Pedro ZM, Casas JA, et al. Preparation of magnetite-based catalysts and their application in heterogeneous fenton oxidation – a review. Appl Catal B Environ. 2015;176-177:249–265.
[22] Azcona P, Zysler R, Lassalle V, et al. Simple and novel strategies to achieve shape and size control of magnetite nanoparticles intended for biomedical applications. Colloids Surf A Physicochem Eng Asp. 2016;504:320–330.
[23] Chen L, Zhou CH, Fiore S, et al. Functional magnetic nanoparticle/clay mineral nanocomposites: preparation, magnetism and versatile applications. Appl Clay Sci. 2016;127-128:143–163.
[24] Khanna L, Verma NK, Tripathi SK, et al. Burgeoning tool of biomedical applications - superparamagnetic nanoparticles. J Alloys Compd. 2018;752:332–353.
[25] Jiang W, Zhang X, Gong X, et al. Sonochemical synthesis and characterization of magnetic separable Fe3O4–TiO2 nanocomposites and their catalytic properties. Int J Smart Nano Mater. 2010;1(4):278–287.
[26] Omidi F, Behbahani M, Khadem M, et al. Application of ultrasonication for facilitating the extraction of hippuric acid and methyl hippuric acid in real samples using Fe 3 O 4 @SiO 2 @sodium dodecyl sulfate: experimental design methodology. Anal Methods. 2018;10:4588–4595.
[27] Zhou K, Zhou X, Liu J, et al. Application of magnetic nanoparticles in petroleum industry: a review. J Pet Sci Eng. 2020;188:106943.
[28] Sobhi HR, Ghambarian M, Esrafili A, et al. A nanomagnetic and 3-mercaptopropyl-functionalized silica powder for dispersive solid phase extraction of Hg(II) prior to its determination by continuous-flow cold vapor AAS. Microchim Acta. 2017;184(7):2317–2323.
[29] sedghi R, Shojaee M, Behbahani M, et al. Application of magnetic nanoparticles modified with poly(2-amino thiophenol) as a sorbent for solid phase extraction and trace detection of lead, copper and silver ions in food matrices. RSC Adv. 2015;5(83):67418–67426.
[30] Bagheri A, Behbahani M, Amini MM, et al. Preconcentration and separation of ultra-trace palladium ion using pyridine-functionalized magnetic nanoparticles. Microchim Acta. 2012;178(3–4):261–268.
[31] Abdollahi H, Maleki S, Sayahi H, et al. Superadsorbent Fe3O4-coated carbon black nanocomposite for separation of light rare earth elements from aqueous solution: GMDH-based neural network and sensitivity analysis. J Hazard Mater. 2021;416:125655.
[32] Sobhi HR, Ghambarian M, Behbahani M, et al. Application of dispersive solid phase extraction based on a surfactant-coated titanium-based nanomagnetic sorbent for preconcentration of bisphenol A in water samples. J Chromatogr A. 2017;1518:25–33.
[33] Kutluay S. Excellent adsorptive performance of novel magnetic nano-adsorbent functionalized with 8-hydroxyquinoline-5-sulfonic acid for the removal of volatile organic compounds (BTX) vapors. Fuel. 2021;287:119691.
[34] Şahin Ö, Kutluay S, Horoz S, et al. Fabrication and characterization of 3,4-diaminobenzophenone-functionalized magnetic nanoadsorbent with enhanced VOC adsorption and desorption capacity. Environ Sci Pollut Res. 2021;28(5):5231–5253.
[35] Ece MŞ. Synthesis and characterization of activated carbon supported magnetic nanoparticles (Fe O4/AC@SiO @Sulfanilamide) and its application in removal of toluene and benzene. Colloids Surf A Physicochem Eng Asp. 2021;617:126231.
[36] Liu Z, Du Z, Zou W, et al. Easily collected nano-absorbents for carbon dioxide capture. Chem Eng J. 2013;223:915–920.
[37] Li W, Wu J, Lee SS, et al. Surface tunable magnetic nano-sorbents for carbon dioxide sorption and separation. Chem Eng J. 2017;313:1160–1167.
[38] Karimi Darvanjooghi MH, Pahlevaninezhad M, Abdollahi A, et al. Investigation of the effect of magnetic field on mass transfer parameters of CO 2 absorption using Fe 3 O 4 -water nanofluid. AIChE J. 2017;63:2176–2186.
[39] Shen X, Du H, Mullins RH, et al. Polyethylenimine applications in Carbon Dioxide capture and separation: from theoretical study to experimental work. Energy Technol. 2017;5(6):822–833.